A preliminary evaluation of the performance parameters of point absorbers for the extraction of wave energy

J. B. Valencia & C. Guedes Soares
Centre for Marine Technology and Ocean Engineering (CENTEC), Instituto Superior Técnico Universidade de Lisboa, Lisbon Portugal

ABSTRACT**:** This present paper preliminarily assesses the performance parameters of point absorber wave energy converter with selected bottom shapes in specific geographic locations and considering viscous effects. Three geometries of cylindrical, conical and hemispherical base are modelled as axi-symmetric bodies having common displacement and stiffness power take-off set to zero. In regular shallow water waves, each model is compared themselves at different ratios and angles as the case may be. The three bodies are scaled to the prototype size and under conditions of regular deep water waves, the hydrodynamic and energy performance parameters are compared and optimized. For an irregular waves marine environment, four geographic zones are chosen to evaluate the performance of the three WECs. For this purpose, the following metrics are calculated: mean annual power flux, mean annual energy production and the mean annual capture width, considering the scenarios: (i) variable power take-off damping (ii) optimal power take-off damping.

1 INTRODUCTION

Numerical modelling is applied from the initial stages of design of a wave energy converter to get an approximation of the hydrodynamic behavior that it has and so understanding how some parameters (the direction of the wave, water depth, wavelength) affect the performance of the mechanical power in the process definition of the concept designs. Numerous studies of single body point absorbers that comparing the absorbed power of axisymmetric geometries were carried out in the last decades. Pioneering research which analyzed cylindrical floating buoys with conical and hemispherical bottom in heave motion were done by (De Backer et al., 2007) simulated with WAMIT and (Pastor and Liu, 2014) using Ansys Aqwa. Both papers follow a similar methodology to calculate the energy absorption of the irregular waves. A hydrodynamic research of moored floating bodies which have their submerged part with shapes of cosine and spherical type was developed by (Berenjkoob et al., 2018) using Ansys Aqwa. The viscous effects were included by (Bhinder et al., 2011) using CFD code Flow 3D verifying for a fully submerged cylinder that there is a notable diminution of the power function and the mean annual energy production. (Tom and Yeung, 2013) investigated the differences in hydrodynamic performance between flat and hemispherical bottom floaters using a CFD in-house code. A approach applied by (Zhou et al., 2020) to speed up the calculations in the frequency domain of the device converter performance in viscous conditions is to use the BEM codes to solve the motion equation in inviscid fluid and to add viscous corrections which can be obtained via the decay test. Considering this last focusing and with the objective of obtaining the performance parameters on the European Atlantic coast, in the present work a step-by-step study was developed in the frequency domain describing the procedure in detail with the necessary simplifications. The potential flow equations were solved using WAMIT. Albeit the response amplitude operator RAO can be obtained directly from the BEM solver, it was calculated from the heave body motion equation $\hat{z}$ divided by the incident wave amplitude ζ_a to be able to introduce the viscous term. Next, the WEC performance parameters of the geometries in study in regular and irregular waves are obtained and hydrodynamically compared. Although this domain gives an useful overview of the optimal dynamics of WEC, will be necessary to perform a study future in the time domain to introduce non linear variables and to compare that with the results of a CFD research.

2 THEORETICAL BACKGROUND

2.1 *Dynamic of the floater*

Using the linear wave theory, the frequency domain equation to the heaving free-floating body is derived:

$$\{-\omega^2(m+\mathrm{a})+i\omega(b)+(k)\}\hat{z}=\hat{f}_e \quad (1)$$

The coefficients added mass a, potential damping b and hydrostatic restoring k can be obtained analytically for

simple geometries, but when complexity increases the BEM solvers are needed.
If it is considered the heaving device doesn't haves mooring, the PTO force $\hat{f}_{pto}$ and the viscous force $\hat{f}_v$ are linear and included with a velocity $\hat{v} = i\omega\hat{z}$:

$$\hat{f}_{pto} = -b_{pto}\hat{v} - k_{pto}\hat{z} \quad (2)$$

$$\hat{f}_v = -b_v\hat{v} \quad (3)$$

Then the motion equation is:

$$\{-\omega^2(m + \mathrm{a}) + i\omega(b + b_v + b_{pto}) + (k + k_{pto})\}\hat{z} = \hat{f}_e \quad (4)$$

Equation 4 represents the mass-spring-damper system model for a single DOF WEC body, see Figure 1.

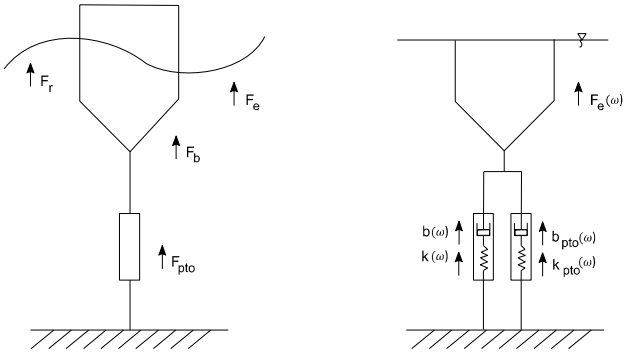

Figure 1 - Heaving WEC model including radiation, exciting, buoyancy and PTO force.

A summary of the device performance equations used in regular waves is shown (Thomas, 2008):

Response amplitude operator [m/m]

$$RAO = |\hat{z}|/\zeta_a \quad (5)$$

Power absorbed [kW]:

$$\bar{P}_{a,reg} = \frac{1}{2}\omega^2 b_{pto}|\hat{z}|^2 \quad (6)$$

Power function [kW/m^2]

$$\bar{p}_{reg} = \frac{1}{2}\omega^2 b_{pto} RAO^2 \quad (7)$$

Capture width [m]

$$L_{w,reg} = \bar{P}_{a,reg}/\bar{P}_{w,reg} \quad (8)$$

Capture width ratio [-]

$$CWR_{reg} = L_{w,reg}/L_c \quad (9)$$

Also the wave energy flux per meter wave-front for regular waves (Shaw, 1982) is expressed in [kW/m].

Deep-water waves:

$$\bar{P}_{w,reg} = \frac{\rho g^2 \zeta_a^2}{4\omega} \quad (10)$$

Shallow-water waves:

$$\bar{P}_{w,reg} = \frac{1}{2}\rho g^{1.5}\zeta_a^2\sqrt{h} \quad (11)$$

Similarly, the irregular version for deep waters [kW/m]:

$$\bar{P}_{w,irr} = \frac{\rho g^2}{64\pi} H_{m0}^2 T_e \quad (12)$$

where H_{m0} and T_e are the spectral moments: significant wave height and energy period respectively, derived from Jonswap spectrum.

In point absorbers, the maximum energy extraction usually will occur when system natural oscillations ω_o approach or equal the frequency of incoming waves ω_i, be these of regular or irregular type. This is the resonance phenomenal and the frequency $\omega_r = \omega_o = \omega_i$ is only reached when the velocity of the oscillating body $\hat{v}$ is in phase with the excitation force $\hat{f}_e$, from which can be obtained the resonance frequency ω_r under two situations: the PTO force includes or omits, the spring coefficient k_{pto}.

$$\omega_r = \omega_o = \sqrt{\frac{k + k_{pto}}{m + \mathrm{a}}} \quad (13)$$

Damping passive control approach $k_{pto} = 0$ and the maximization of mean power (equation 6) is affected considering that the average absorbed power only depends on the PTO damping $\bar{p}_{reg} = \bar{p}_{reg}(b_{pto})$. Thus, deriving $\frac{\partial \bar{p}_{reg}}{\partial b_{pto}} = 0$, it results the optimal damping coefficient:

$$b_{opt} = b_{pto} = \sqrt{b^2 + \frac{1}{\omega^2}[-\omega^2(m + \mathrm{a}) + k]^2} \quad (14)$$

If one introduces equation 13 in equation 14, the optimal condition in resonance is:

$$b_{pto} = b \quad (15)$$

Direct consequents of the damping PTO control, are the expressions to calculate the maximum theoretical mean power of a single mode WEC:

$$\bar{P}_{\mathrm{m}} = \frac{|\hat{\mathrm{f}}_{\mathrm{e}}|^2}{8\mathrm{b}_{\mathrm{opt}}} \quad (16)$$

The final aim of the development of WEC concept and its numerical stages is the estimation of levelized cost of energy (LCoE), that involve a complex quantity of variables and uncertainties: (a) capital cost (device cost, installation, production) (b) operation cost (maintenance, insurance) (c) mean annual energy production MAEP, all them depend directly of the PTO system and in this study will be used a simplified linear version as described in equation 2.

2.2 *Performance of the WEC*

The scatter diagram represents the wave climate of a geographical area during a time period (usually tens of years) and considering the wave directionality, it is normally organized in a two-dimensional matrix $C(H_s, T_e)$. The vertical and horizontal references correspond to the wave significative heights H_s and time periods T_e respectively. Each cell (bin) of this matrix represents the relative frequency of occurrence f_{H_s,T_e} of the respective combination (H_s, T_e). It both span in constant way, H_s in meters, T_e in seconds and depend on the size of the zone in study. The matrix $C(H_s, T_e)$ meets the next condition: $\sum_{i=1}^{N} C_i = 1$, where N is the number of sea-states.

The mean annual wave power flux (MAPF) per meter wave-front [kW/m], may be calculated by summing over all energy fluxes of an element-wise matrix multiplication between $\bar{P}_{w,irr}$ transported in each sea state defined in equation 12 and the probability of occurrence $C(H_s, T_e)$ (Beels et al., 2007).

$$MAPF = \sum_{H_s} \sum_{T_e} C(H_s, T_e) \odot \bar{P}_{w,irr}(H_s, T_e) \quad (17)$$

The performance matrix, is the representation of the mechanical power ideally extractable in [kW] by the WEC device. This involves all the components that participate actively on the process of primary conversion energy that varies with sea state and falls mainly on the PTO machine. Each element of the matrix is calculated by the following formula:

$$\bar{P}_{a,irr}(H_s, T_e) = 2 \int_0^{\infty} \bar{p}_{reg}(\omega) S_{\zeta}(\omega) d\omega \quad (18)$$

where $\bar{p}_{reg}$ is the power function defined in equation 7, and S_{ζ} is the Jonswap energy spectrum. However, it can be considered an additional power matrix that represents the absorbed power of a specific area and to obtain it, $\bar{P}_{a,irr}$ is multiplied element-wise by the probability of each sea state.

$$PM_{H_s T_e} = C(H_s, T_e) \odot \bar{P}_{a,irr}(H_s, T_e) \quad (19)$$

The mean annual energy production (MAEP) is the total energy produced over an one-year period [kW-h], that can be estimated in its form simpler (Kofoed and Folley, 2016):

$$MAEP = \sigma \sum_{H_s} \sum_{T_e} PM(H_s, T_e) \quad (20)$$

where $PM(H_s, T_e)$ is the power matrix obtained in equation 19, σ is the numerical factor $24x365$ hours/year (Gregorian year) that assume the ideal conditions of work of generate energy uninterruptedly with 100% of availability.

The mean annual capture width (MACW) is the same concept of capture width [m] of the equation 8, but this time using the parameters MAEP and MAPF as variables:

$$MACW = \sigma^{-1} \frac{MAEP}{MAPF} \quad (21)$$

If this value is divided by the characteristic length L_c in meters, a nondimensional parameter is obtained: mean annual capture width ratio (MACWR).

3 WAMIT MODELLING

To validate our subsequent hydrodynamics calculations, the results will be compared with numerical data from (Falnes, 2002) for a floating cylinder. WAMIT has two approaches for get the hydrodynamic coefficients: low order LO and high order HO analysis (WAMIT Inc, 2013).

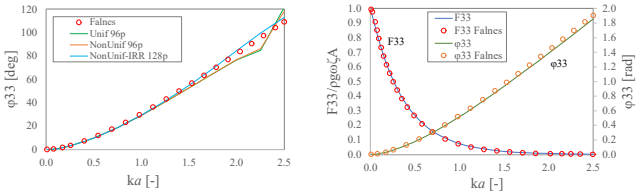

Figure 2 – LO / HO discretizations (a) Phase lag (b) F_{33} and phase

For LO validation with Falnes curves, Figure 2(a) considers a discretization with uniform meshing Unif, non-uniform meshing (cosine spacing) NonUnif and non-uniform meshing under the irregular frequencies removal NonUnif-IRR. For a similar HO validation curves, Figure 2(b) considers a meshing with cosine space distribution with irregular frequency removal.

With a simple visual analysis in LO, it is clear that the non uniform version with irregular frequency removal is the best fit. It was also verified in the HO method. To quantify that, it was done a convergence study on heave mode with an incremental mesh refinement on a cylinder with a radius of 5 meters and heading angle of 45 degrees.

The low order convergence is soft and was done with discretization of 32 and 1568 panels, as minimal and maximum values by quadrant. See Figure 3(a).

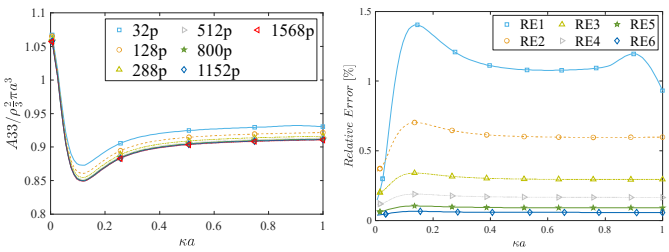

Figure 3 - Heave convergence LO (a) Added mass (b) Relative error

The relative error tends to the zero percent with the higher value of the panelization. See Figure 3(b).

A comparison among both approaches is made. In the Figure 4(a) is visible that HO convergence is fastest and in all cases the discretization ILOWHI-1 of 128 and 288 panels is under 0.5% relative error compared with the best value of the low order discretization. See Figure 4(b).

The value of 128 panels was chosen for subsequent calculations because in practical purposes the BEM solver runs faster.

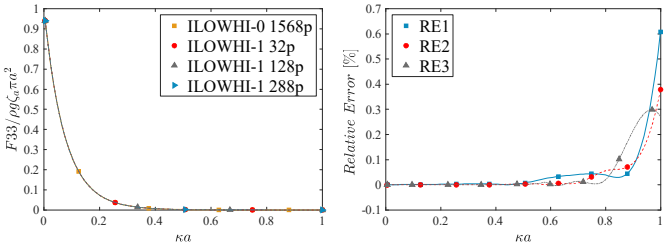

Figure 4 - Heave convergence HO (a) Exciting force β=45° (b) Relative error

4 PERFORMANCE IN REGULAR WAVES

The geometrical bodies in this study have as common base the ratio $r = a/d$. Figure 5(a) cylinder with a and d as the *radius* and *draft* respectively from which the expressions are deducted for the *equivalents drafts* of the others WECs devices: Figure 5(b) cylinder with conical base $(d_1 + d_2)$ and the Figure 5(c) cylinder with hemispherical base $(d'_1 + d'_2)$.

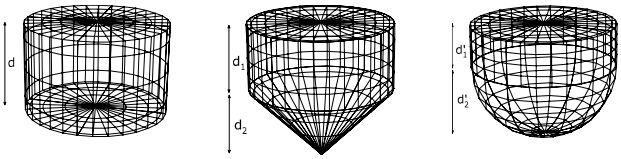

Figure 5 - Axi-symmetrical bodies (a) Cylindrical (b) Conical (c) Hemispherical

The draft formulas that correspond to each geometry with the condition $d = 1$ are shown in Table 1.

Table 1 – Equivalent draft formulas

BCyl	BCone	BHemis
d	$d_1 = d(1 - \frac{1}{3}\frac{r}{\tan(\propto)})$	$d'_1 = d(1 - \frac{2}{3}r)$
	$d_2 = \frac{d \cdot r}{\tan(\propto)}$	$d'_2 = a$

4.1 *Dimensions and characteristics*

The input's parameters of design are: BCyl(a, d), BCone$(a, d_1, d_2, \propto)$ and BHemis(a, d'_1, d'_2) see Table 2, with which can be obtained derived parameters as water plane area, submerged volume, the hydrostatic restoring coefficient, among others.

Table 2 – Model dimensions with scale=0.2

BCyl	r = 0.8	r = 1.2	r = 1.4
a	0.8000	1.2000	1.4000
d	1.0000	1.0000	1.0000

BCone 45°			
r = 0.8	α = 45°	α = 60°	α = 75°
a	0.8000	0.8000	0.8000
d1	0.7333	0.8460	0.9285
d2	0.8000	0.4619	0.2144

BHemis	r = 0.8	r = 1.2	r = 1.4
a	0.8000	1.2000	1.4000
d1	0.4667	0.2000	0.0667
d2	0.8000	1.2000	1.4000

The values of the environmental constants used on the calculations are shown in the Table 3.

Table 3 – Environment constants

	Gravity	9.81 m/s^2
	Shallow water	Deep water
Wave amplitude	0.1 m	1 m
Depth	15 m	500 m
Density	1000 kg/m^3	1025 kg/m^3

The viscous correction data was obtained from (Zhou et al., 2020), see table 4.

Table 4 – Models' viscous damping [kg/s]

BCyl	BvisT	Binv	Bvis	Fv
0.8	1165	453	712	2.57
1.2	3378	1766	1612	1.91
1.4	4880	2912	1968	1.68

BCone 45°	BvisT	Binv	Bvis	Fv
0.8	558	468	90	1.19
1.2	2145	1967	178	1.09
1.4	3507	3435	72	1.02

BHemis	BvisT	Binv	Bvis	Fv
0.8	488	485	2.5	1.01
1.2	2048	1988	60	1.03
1.4	3675	3588	87	1.02

B_{visT} is the total viscous damping, B_{inv} is the inviscid damping, B_{vis} is the correction damping and F_v is the non-dimensional coefficient viscous damping correction.

The viscous damping was directly applied to the scale of the models and then scaled using the values $[B_{visT}, B_{inv}, B_{vis}]$ x scale$^{2.5}$ for the prototype body.

The expressions for the natural frequency ω_n of the three free floating bodies are given next and include μ_{33} the non-dimensional added mass, g the gravity and the drafts before calculated.

Table 5 - Natural frequency formulas

BCyl	BCone	BHemis
$\omega_n^2 = \frac{g}{d[1+\mu_{33}(\omega_n)]}$	$\omega_n^2 = \frac{g}{[d_1 + \frac{1}{3}d_2][1+\mu_{33}(\omega_n)]}$	$\omega_n^2 = \frac{g}{[d'_1 + \frac{2}{3}d'_2][1+\mu_{33}(\omega_n)]}$

Natural frequency ω_n [rad/s], calculated iteratively for the scenarios simulated:

Table 6 – Natural frequencies [rad/s] for models scale 1/5

BCyl	r	0.8	1.2	1.4
	ωn	2.607	2.449	2.381
BHemis	r	0.8	1.2	1.4
	ωn	2.784	2.669	2.620
BCone	r=0.8/∝	45°	60°	75°
	ωn	2.773	2.712	2.658

Table 7 - Natural frequencies [rad/s] for prototypes

$r = 0.8$	BCyl	BCone 45°	BHemis
ω_n	1.166	1.240	1.245

4.2 *Shallow water regular waves simulations*

4.2.1 *WEC cylindrical base (BCyl)*

Simulations of *BCyl* models with ratios $r = \{0.8, 1.2, 1.4\}$ are shown. Using programming was possible to add the PTO force with a damping boot $b_{pto} = 400$ kg/s, and besides the viscous damping from Table 4.

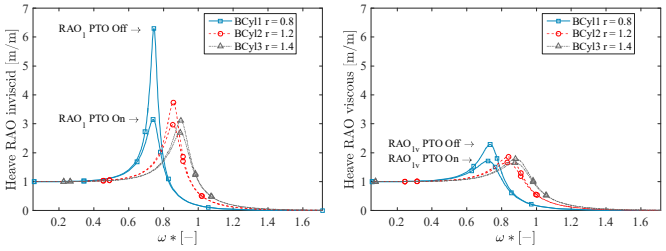

Figure. 6 - BCyl RAO with PTO on / off (a) Inviscid fluid (b) Viscous fluid

It is visible a clear decrease of three times its peak value when the PTO is applied under the inviscid condition Figure 6(a). Then a new drop of almost two times the value of peak occurs, by the effect of the viscosity in the captor BCyl1 Figure 6(b). This situation of peaks falling is repeated in each geometry with smaller impact and it is evident that the viscous correction affects notably to the more slender body, i.e. the one with less ratio. Also, the calculated resonant frequencies of the captors in inviscid fluid $\omega = \{2.591, 2.440, 2.370\}$ [rad/s], decrease when is considered the viscous case $\omega = \{2.530, 2.380, 2.320\}$ [rad/s].

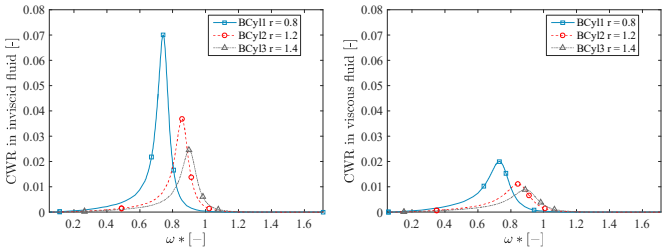

Figure 7 - BCyl CWR (a) Inviscid fluid (b) Viscous fluid

Figure 7(a) shows the capture width ratio CWR for the characteristic length $L_c = [0.8, 1.2, 1.4]$. The unevenness in the peaks is notable in ideal fluid due to the ratios of the bodies, and decreases abruptly under viscous regime Figure 7(b), being the most affected, the one that has less ratio.

As expected, for the low boot damping PTO used, the resonant frequencies coincide with those of the absorbed power, in inviscid or viscous fluid.

4.2.2 *WEC conical base (BCone)*

Simulations of the three *BCone* models, with ratios $r = \{0.8, 1.2, 1.4\}$ and half apex angles $\alpha = \{45°, 60°, 75°\}$ are carried out. (Plots with $r = \{1.2, 1.4\}$ don't are shown.)

Figure 8(a) show the behavior of the RAO PTO-on curves for BCone with ratio: r= {0.8} and different half apex angles $\alpha = \{45°, 60°, 75°\}$, in an inviscid fluid. Clearly is appreciated in the resonant frequency region, the shift of the peaks when the angle α rises, being the BCone 75°, the one with the highest response amplitude.

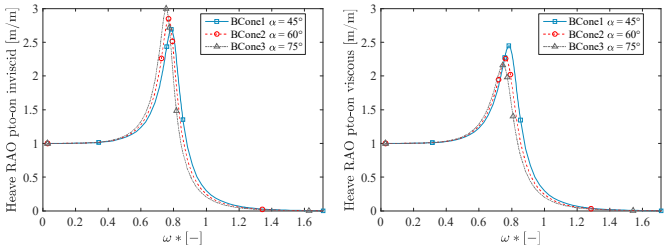

Figure 8 - BCone RAO (a) Inviscid fluid (b) Viscous fluid

Figure 8(b) shows the viscous version, where the order of the peaks is altered and the viscous correction affects notably the geometry with greater conical angle. When comparing the three bodies, it is verified that the fall of the peaks increases when the ratio also increases.

Figure 9(a) shows that Bcone1 75° has the greatest capture width ratio, still when there is a noticeable peak decrease related to ratio increase.

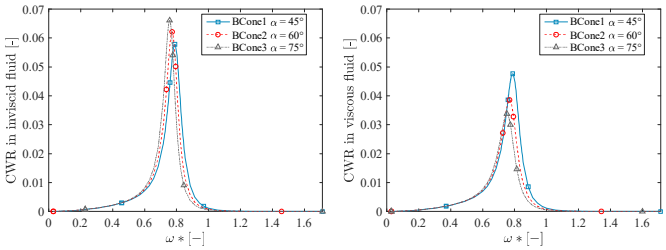

Figure 9 - BCone CWR (a) Inviscid fluid (b) Viscous fluid

In viscous conditions Figure 9(b), the smallest peak becomes the largest and the order of the peak's size is altered but maintaining frequencies coverage.

4.2.3 *WEC hemispherical base (BHemis)*

Simulations of the three *BHemis* models, with ratios $r = \{0.8, 1.2, 1.4\}$ are carried out.

Figure 10(a) shows that the more slender body has the highest response and that due to the viscous effects are very small, the curves almost overlap with the potential version.

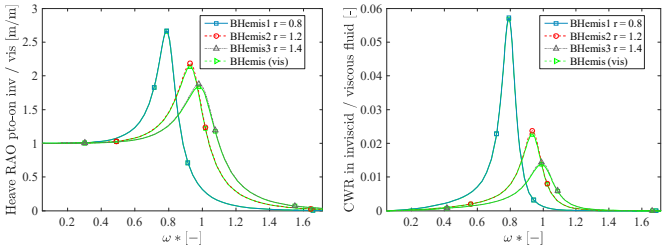

Figure 10 - BHemis inviscid / viscous fluid (a) RAO (b) CWR

Figure 10(b) similarly, due to that the viscous coefficient is close to 1 in each ratio, their effects are very smalls and the curves overlap. A small difference near to the peaks of BHemis2 and BHemis3 is shown. Like before, the slender body has the best performance in the energy's capture.

4.3 *Deep water regular waves simulations for prototypes bodies*

For study the influence of the geometry, three WEC prototypes are compared: *BCyl*, *BCone* ($\propto = 45°$), *BHemis*, with ratio $r = 4\ m$, Other scaled magnitudes are the PTO damping boot 2.236x10^4 kg/s, the hydrostatic restoring coefficient 5.053x10^5 N/m.

The inviscid response Z of the vertical oscillation Figure 11(a) is more pronounced for the BCyl body (aprox. 3.15m). The other responses of BCone 45° and BHemis, overlap and are lower (aprox. 2.6m). A situation a bit more realistic is appreciated in the Figure 11(b) where the BCyl's peak decreases abruptly to almost half of its original value. BCone 45° decreases its peak by only some centimeters and BHemis keeps almost the same position due to the low viscosity for this geometry.

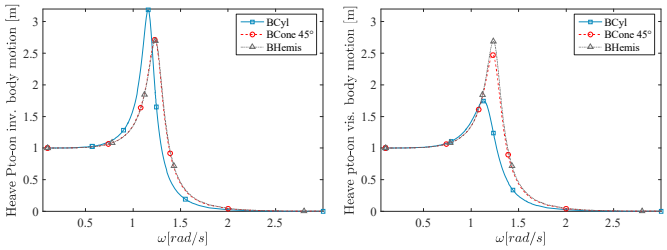

Figure 11 - Three bodies, heave motion Z (a) Inviscid fluid (b) Viscous fluid

Simulations of the theoretical maximal power of absorption P_m and the absorbed power $\bar{P}_a$ together under inviscid and viscous fluid, are carried out.

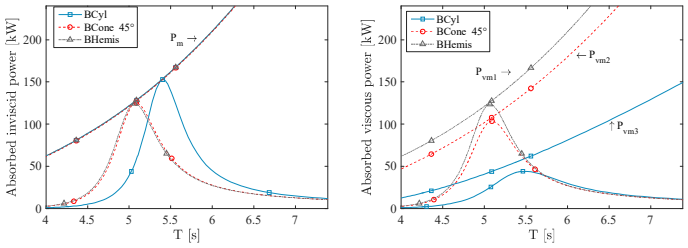

Figure 12 - Three bodies, power absorbed $\bar{P}_a$(a) Inviscid fluid (b) Viscous fluid

In Figure 12(a) is observed that the three bodies get to reach the maximal power, that is a common curve. Figure 12(b) shows that each of the three geometries has a different maximal power and that depending on the value of the viscous coefficient, the curves move away or closer.

The best performance is observed when the BCyl body is in an inviscid regime but in the viscous frame the best one is the BHemis body even than BCone 45°.

When the equation 15 is introduced in the power equations, it brings the optimized power version $\bar{P}_{opt}$.

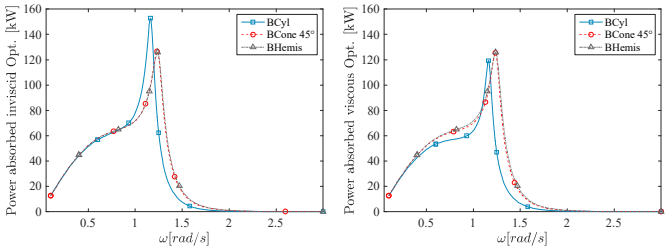

Figure 13 - Three bodies, optimal power $\bar{P}_{opt}$ (a) Inviscid fluid (b) Viscous fluid

At first sight, the Figure 13(a) and Figure 13(b), are similar to the previous plots near to the peaks but they are much different at the spectral low band, giving additional criteria to choose the best WEC. BHemis has slightly better performance in absorbed power over BCone under optimal conditions.

Figure 14(a) shows that the BCyl has the highest value of CWR but a smaller value of frequency range captured compared to the others bodies (under inviscid conditions).

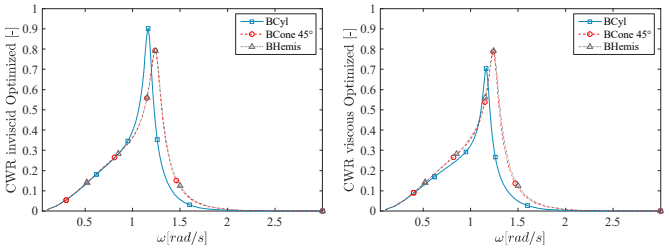

Figure 14 - Three bodies, optimal capture width ratio CWR_{opt} (a) Inviscid fluid (b) Viscous fluid

Figure 14(b) shows that under viscous effects, the peak decreases strongly in the BCyl body and the BCone 45° and BHemis has a similar behavior, however the best performance pertain to the BHemis device because it is lightly better in captured frequencies range and the CWR parameter. Also it has the less viscous dissipation.

5 PERFORMANCE IN IRREGULAR WAVES

5.1 Input environment's parameters

The European Atlantic coast was chosen as the study area. Scatter tables of four geographical areas (Emec, Yeu, Lisbon, Belmullet) were processed and the data files obtained from (LHEEA, 2017). The observation period is assumed to be obtained in an annual period (Pontes, 1998).
The next step is to verify if they actually represent the correct values of the respective energy resource, (this validation is independent of the calculation of the power matrices) which implies the all have the energy spectrum calibrated. For to check so, simulations of some representative sea states of the north sea (De Backer et al., 2007) were done using the Jonswap spectrum.

Sea State	Hs [m]	Tp [s]
1	1.25	6.7
2	1.75	7.4
3	3.25	8.81

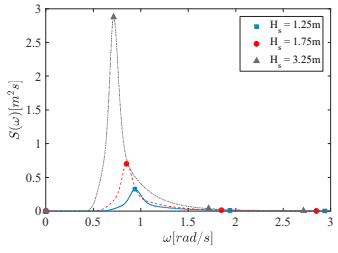

Figure 15 - Typical Jonswap states for the north sea area

Next, using the equation 17, it is calculated the mean annual wave power flux $MAPF$ per meter wave front [kW/m] for each site location (see Table 8). They are compared to the results of (Babarit et al., 2012), that considers the three common values of frequency spreading factor $\gamma = [1, 3.3, 7]$, referred to the Jonswap spectrums [wind sea, typical, long Atlantic swell].

Table 8 - Sites location wave energy resource (kW/m)

Country	Location	Water depth [m]
Scotland	059° 00,000'N - 003° 66,000'W	50
France	046° 40,000'N - 002° 25,000'W	47
Portugal	039° 00,000'N - 012° 00,000'W	100
Ireland	054° 00,000'N - 012° 00,000'W	100

Site	γ = 1	γ = 3.3	γ = 7
Emec	22.19	23.36	24.06
Yeu	25.78	27.13	27.96
Lisbon	36.17	38.09	39.25
Belmullet	77.75	81.88	84.38

5.2 WECs metrics with Bpto variable

In this scenario (case i), the PTO damping coefficient *Bpto* that maximize the energy performance in each site is optimized. The chosen values are powers of ten multiplied by the damping boot. The PTO damping range is: [10^0 10^1 10^2 10^3 10^4 10^5] x BptoZo kg/s, with BptoZo = 2.2 x10^4 kg/s.

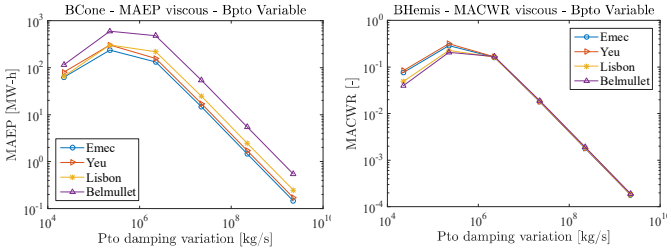

Figure 16 - PTO damping variation (a) MAEP (b) MACWR

It is observed that for the three energy devices, with the PTO damping 10 x BptoZo, the MAEP and MACWR maximum is obtained (Figure 16 (a) and (b) are in logarithmic scale).
The absorbed power matrix was calculated for the areas and geometries under study. These results were multiplied by the respective energy resource occurrence matrices, as indicated in equation 20 to obtain the MAEP of each energy converter device.
If the MAEP is divided between the energy resource and the characteristic length, as the equation 21 shows, the mean annual capture width ratio MACWR is obtained (expressed as a percentage for better visibility). The two performance parameters for the devices under study are shown in Table 9.

Table 9 - Performance metrics for WECs with Bpto variable

BCyl	Bpto variable			
	MAEP [MW-h/year]		MACWR [%]	
	inv	vis	inv	vis
Emec	234.4	208.3	28.64	25.45
Yeu	299.8	266.0	31.53	27.98
Lisbon	301.4	273.9	22.58	20.52
Belmullet	594.1	547.3	20.71	19.07

BCone	Bpto variable			
	MAEP [MW-h/year]		MACWR [%]	
	inv	vis	inv	vis
Emec	236.1	235.7	28.84	28.81
Yeu	301.7	301.3	31.74	31.69
Lisbon	301.9	301.5	22.62	22.59
Belmullet	593.8	593.3	20.70	20.68

BHemis	Bpto variable			
	MAEP [MW-h/year]		MACWR [%]	
	inv	vis	inv	vis
Emec	236.542	236.540	28.9043	28.9041
Yeu	302.369	302.366	31.8016	31.8014
Lisbon	302.175	302.173	22.6410	22.6409
Belmullet	594.080	594.077	20.7069	20.7068

5.3 *WECs metrics with Bpto optimal*

For this scenario (case ii) the absorbed power for each sea state is optimized using the damping passive control of the equation 14. The results of the performance parameters obtained as in section 5.2 are shown in Table 10:

Table 10 - Performance metrics for WECs with Bpto optimal

BCyl	Bpto optimal			
	MAEP [MW-h/year]		MACWR [%]	
	inv	vis	inv	vis
Emec	326.0	276.8	39.84	33.82
Yeu	405.8	343.0	42.68	36.07
Lisbon	451.0	398.3	33.79	29.84
Belmullet	924.8	831.6	32.23	28.99

BCone	Bpto optimal			
	MAEP [MW-h/year]		MACWR [%]	
	inv	vis	inv	vis
Emec	327.4	326.7	40.01	39.92
Yeu	407.8	406.9	42.89	42.80
Lisbon	454.5	453.8	34.05	34.00
Belmullet	933.7	932.4	32.54	32.50

BHemis	Bpto optimal			
	MAEP [MW-h/year]		MACWR [%]	
	inv	vis	inv	vis
Emec	328.000	327.996	40.0800	40.0796
Yeu	408.604	408.599	42.9749	42.9744
Lisbon	454.993	454.990	34.0913	34.0910
Belmullet	934.373	934.367	32.5679	32.5677

For the case (i), the energy extraction is higher for BHemis and BCone in all sites, if the viscous fluid is considered. In the case of inviscid fluid, the situation is similar except for Belmullet, by tenths, due to the statistical variability of the results. For the case (ii), BHemis and BCone continues to be the WEC with the best productivity in an inviscid and viscous fluid when compared in each site or in all sites, due to its less viscous effects.

In all cases, the performance of each device in the four sites projects an ascending linear relationship for the MAEP, as the energy resource increases Figure 17. Indeed, it seems reasonable to expect greater energy extraction in the sites with the highest energy resources, taking into account that only one technology is being modeled. Also can be inferred that there is a limit of absorbed power (Babarit and Hals, 2011).

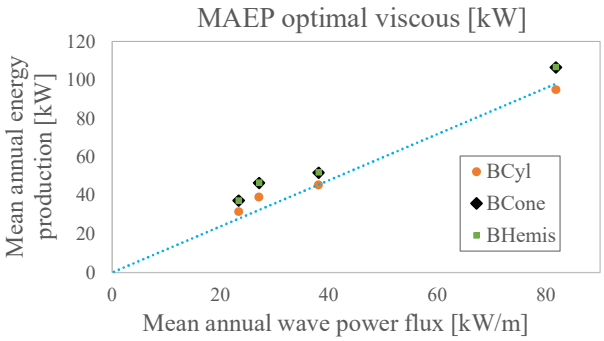

Figure 17 - MAEP versus energy resource sites

Take into account that when two sites as Emec and Yeu, with similar level of depth and energy resource are compared, the second one is more productive. One explanation could be that around the island of Yeu, longer wavelengths are more common, whose magnitude is of the order of the square of the period ~ $1.56T^2$.

6 CONCLUSIONS

With numerical validation, it was concluded that WAMIT higher order method is the most efficient for evaluating geometries with symmetries, given its rapid implementation and precise convergence.

In regular waves, from the individual study of each axisymmetric geometry model considering constant damping PTO 400 kg /s, it was concluded that:
For BCyl and BHemis under inviscid conditions, the shift of the resonance frequencies towards the high frequency zone is directly related to the increase in the dimensions of the buoy. For BCone, the shift of the resonance frequencies towards the low frequency zone is directly related to the increase of the half apex angle when the displacement is kept constant. This is explained by the influence that the hydrodynamic parameters have on the resonance equation 13. Considering viscous conditions for BCyl and BHemis there is a natural decrease in the RAO maximums but a pronounced drop in the more slender bodies (less ratio) and a decrease in the resonance frequencies. For BCone there is a decrease of resonant responses that affects notably the geometry with greater conical angle and also the peaks order is altered, when the displacement held constant.

In regular waves, were compared the performance parameters of three axisymmetric geometries prototype optimized considering constant damping PTO ~ 10^4 kg/s and their viscous corrections. After was concluded that: BCone and BHemis have the best capture width ratio CWR and power absorbed with the highest

resonant frequencies although the second one body has slightly better performance.

The wave power available in regular deep water waves and shallow water waves has an evident impact on results obtained for CWR of the analyzed geometries having their origin in the celerity embedded in equation 10 and equation 11 where the first one has a wave length dependency and second one only depend of water depth.

It is evident a pronounced difference in the capture of energy from regular shallow waters and deep waters, mainly due to the first one doesn't depend of the wave frequency.

In irregular waves of four geographical areas were compared the performance parameters MAEP and MACWR of three axisymmetric geometries prototype under viscous effects, considering: (i) A variation of damping PTO seeking to maximize energy performance in each site. (ii) An optimized PTO damping coefficient seeking for the best performance for each sea state. After was concluded that:

Under optimal conditions, there is a linearity related to energy resources. That is, if the productivity of BCyl, BCone and BHemis is analyzed in all the sites, a linear correlation with the increase of the energy resource is visible and it can be inferred that there is a limit of absorbed power. The designs with the highest energy productivity are BCone 45° and BHemis, considering the latter has a slightly better performance, however there are factors that need to be verified for it to be a definitive result.

These factors should be developed in future research and include:

- Viscous corrections must be verified via CFD or laboratory experiments.
- The statistical variability of the scatter tables must be contrasted with time series data.
- Time domain model must be compared.
- Non-linear effects must be included in the numerical model.

REFERENCES

Babarit, A., and Hals, J. (2011). On the maximum and actual capture width ratio of wave energy converters. in *10th European wave energy conference,* (Southampton).

Babarit, A., Hals, J., Muliawan, M. J., Kurniawan, A., Moan, T., and Krokstad, J. (2012). Numerical benchmarking study of a selection of wave energy converters. *Renew. Energy* 41, 44–63. doi:https://doi.org/10.1016/j.renene.2011.10.002.

Beels, C., De Rouck, J., Verhaeghe, H., Geeraerts, J., and Dumon, G. (2007). Wave energy on the Belgian Continental Shelf. in *OCEANS 2007 - Europe*, 1–6.

Berenjkoob, M. N., Ghiasi, M., and Soares, C. G. (2018). Hydrodynamic analysis of different geometries of a wave energy absorber buoy. in *3rd International Conference on Renewable Energies Offshore (RENEW 2018)* Proceedings in Marine Technology and Ocean Engineering.

Bhinder, M., Babarit, A., Gentaz, L., and Ferrant, P. (2011). Assessment of viscous damping via 3D-CFD modelling of a Floating Wave Energy Device. in *9th European Wave and Tidal Energy Conference* (Southampton, United Kingdom).

De Backer, G., Vantorre, M., Banasiak, R., Beels, C., and De Rouck, J. (2007). Numerical Modelling of Wave Energy Absorption By a Floating Point Absorber System. in International Ocean and Polar Engineering Conference. (Lisbon, Portugal), 374--379.

Falnes, J. (2002). *Ocean Waves and Oscillating Systems: Linear Interactions Including Wave-Energy Extraction*. Cambridge University Press.

Kofoed, J. P., and Folley, M. (2016). "Chapter 13 - Determining Mean Annual Energy Production," in *Numerical Modelling of Wave Energy Converters*, ed. M. Folley (Academic Press), 253–266.

LHEEA (2017). LHEEA (last visited Feb. 2017). Available at: https://lheea.ec-nantes.fr/doku.php/emo/ew-tec2015shortcourse/start.

Pastor, J., and Liu, Y. (2014). Frequency and time domain modeling and power output for a heaving point absorber wave energy converter. *Int. J. Energy Environ. Eng.* 5, 101. doi:10.1007/s40095-014-0101-9.

Pontes, M. T. (1998). Assessing the European Wave Energy Resource. *J. Offshore Mech. Arct. Eng.* 120, 226–231. doi:10.1115/1.2829544.

Shaw, R. (1982). *Wave Energy - A Design Challenge*. Wiley.

Thomas, G. (2008). "The Theory Behind the Conversion of Ocean Wave Energy: a Review," in *Ocean Wave Energy: Current Status and Future Prespectives*, ed. J. Cruz (Berlin, Heidelberg: Springer Berlin Heidelberg), 41–91. doi:10.1007/978-3-540-74895-3_3.

Tom, N., and Yeung, R. W. (2013). Performance Enhancements and Validations of a Generic Ocean-Wave Energy Extractor. *J. Offshore Mech. Arct. Eng.* 135. doi:10.1115/1.4024150.

WAMIT Inc (2013). WAMIT v7.0 user manual.

Zhou, B., Hu, J., Sun, K., Liu, Y., and Collu, M. (2020). Motion Response and Energy Conversion Performance of a Heaving Point Absorber Wave Energy Converter. *Front. Energy Res.* 8. doi:10.3389/fenrg.2020.553295.